Femtosecond Chemical Dynamics in Solution: Photodissociation of I_3^-

Uri Banin,[a,b] Ronnie Kosloff,[b] and Sanford Ruhman[a,b]*
Department of Physical Chemistry, [a]Farkas Center for Light-Induced Processes, [b]Fritz Haber Center
for Chemical Reaction Dynamics, The Hebrew University of Jerusalem, 91904 Jerusalem, Israel

(Received 15 March 1993 and in revised form 5 April 1993)

Abstract. We report a study of the UV photolysis of I_3^- in alcohol solutions, using femtosecond time-resolved transient transmission experiments. We interpret our results to indicate that photoexcitation leads to direct formation, within 300 fs, of diiodide ions which are vibrating coherently. The time scales for vibrational dephasing, vibrational relaxation, and reorientation of the fragment ions are 400 fs, 4 ps, and 5 ps, respectively. UV transient transmission experiments were conducted in order to characterize the time scales for recombination. Recombination takes place on several time scales. A fast component is assigned to primary recombination, followed by vibrational relaxation on the ground state of I_3^-. The prominence of this recombination route is found to be strongly dependent on the solvent. Finally, time domain quantum simulation techniques are employed in order to gain insight into the nature of the nascent diiodide vibrational distribution, and to introduce a semiquantitative model for the stage of bond fission for isolated ions.

INTRODUCTION

Recent experiments have convincingly demonstrated the utility of femtosecond laser spectroscopy for the study of intramolecular dynamics in real time. At the expense of certainty concerning the energy content of impulsively photoexcited molecules, intramolecular vibrations and chemical rearrangements can be induced in the form of coherent nuclear motion, and followed in real time by a variety of pump–probe spectroscopies.[1] It is hard to overestimate the potential of this approach to the study of photochemical dynamics in condensed phases. Due to irreversible solvent-induced relaxation, the excess energy imparted on the products is rapidly dissipated. It is therefore impossible to reconstruct the critical stage of bond fission or formation by probing the products after the fact. The rapid rate of solvent-induced electronic dephasing limits the utility of resonance Raman as a method of gaining insight into the course of photoinduced chemical reactions in solution.[2] Only through the application of direct real time spectroscopic probing, with time resolution capable of resolving both intra- and intermolecular motions in the liquid phase, will it be possible to unravel solution chemical dynamics in detail.

The photodissociation of iodine in liquid solutions has served as a model dissociation reaction, and has been studied extensively using ultrafast spectroscopic methods[3] and theoretical modeling.[4] Picosecond time-resolved laser spectroscopy has been used to gain a quantitative picture of solvent caging, curve crossing, geminate recombination, and vibrational relaxation on the X and B states of iodine. Impulsive photoexcitation of iodine solutions on the femtosecond time scale has recently allowed direct observation of coherent intramolecular vibration, dephasing, and predissociation on the B state in a series of solvents.[5]

In the work reported here, we applied femtosecond laser flash photolysis to study the dynamics of triiodide ion photodissociation and recombination in alcohol solutions.[6] The extension of ultrafast investigation of photodissociation in liquids to a triatomic system adds many interesting dynamic observables to the process, while keeping it within the reach of detailed theoretical treatments via molecular dynamics or other techniques.[7] Excess energy deposition into internal motions of the molecular fragment, and its subsequent relaxation into the bulk, are just examples of this dynamical richness. The possibility of coherence propagating from the stage of

---

*Author to whom correspondence should be addressed.

bond fission to product states in isolated molecules has been demonstrated by Zewail and coworkers in their study of HgI_2 photolysis.[8] The molecular ion we are experimenting with here is especially interesting due to the strong interactions between it and the solvent molecules, the dramatic changes in charge distribution following photoexcitation, and the fact that all intramolecular motions of the parent and fragment ions are directly time resolvable with our laser system.

In the following we will present recent results on the photodissociation of triiodide in polar solvents:

$$I_3^- \xrightarrow{h\nu} I_2^-\cdot + I\cdot \qquad (1)$$

Very rapid evolution in the absorption data is interpreted as due to direct bond cleavage within roughly 300 fs. Oscillations and overall decays in the data for the visible and near IR spectral regions, immediately following dissociation, are the signature of coherent vibrational motion and subsequent vibrational population decay in the nascent I_2^- fragments. Photoselective probing methods are applied to detect parent and fragment ion reorientation, and observed optical density variations in the UV are analyzed in terms of various phases of geminate recombination. Finally, time-domain quantum simulation techniques are employed in order to gain insight into the nature of the nascent diiodide vibrational distribution, and to introduce a semiquantitative model for the stage of bond fission for isolated ions.

SPECTROCHEMICAL BACKGROUND

The triiodide ion is linear and symmetric in solution, and stable in many polar solvents.[9] The absorption spectra of triiodide in ethanol consists of two bands whose spectral assignment has been the subject of debate.[10] The most common explanation is that excitation leads to dissociative states correlating with I_2^- $(^2\Sigma_u^+)$ in the ground state, and $I(^2p)$ in either of its lowest spin orbit states.[11] Polarized absorption experiments on I_3^- in crystals proved[10b] that both transitions are polarized parallel to the molecular axis. The first suggestion of the consequences of the primary photochemical step as leading to direct dissociation according to reaction 1 was based on CW scavenging experiments.[12] Later studies, using flash photolysis, provided further evidence for this assumption, through measurements of the decay kinetics at longer times.[13]

Our work is the first attempt to resolve the early time dynamics involving the process of fragment formation. The only existing information relevant to the stage of photocleavage comes from Resonance Raman (RR) spectra, recorded with excitation sources falling within the near UV absorption bands of the triiodide ion. The UV RR spectrum in solution,[14] and in crystal lattices,[15] shows a long progression of the symmetric stretch, indicating that the initial motion on the excited-state potential is predominantly directed along this coordinate. Calculations of the potentials of triiodide have concentrated mainly on explaining the hypervalent nature of the chemical bond in this molecule,[16] and detailed orbital mapping of the ground state shows the excess negative charge to be distributed evenly between the end atoms, while a small positive charge is left on the central atom. We know of a single attempt that has been made to calculate one-dimensional cuts along the symmetric and asymmetric coordinates.[17] The results do not clearly explain why the primary photochemical step should proceed by reaction 1, and the possibility of more than one dissociation channel should be considered. The stabilization energy of the triiodide ion with respect to dissociation into an iodine molecule, and iodide ion in the gas phase, is ~1 eV.[18] We must stress that this result is for the isolated ion, and that in solution the ΔH^0 for this process is considerably lower.[19]

The diiodide radical has been studied in solution,[20] as a color center in crystals,[21] and more recently its photodissociation and recombination have been probed in real time, both in solution[22] and in gas-phase clusters.[23] The electronic absorption spectrum is composed of two bands — one in the near UV, partly overlapping the triiodide absorption spectra, and the other in the near IR centered at ~740 nm in ethanol.[24] This band is very distinct from the I_3^- absorptions, and its temporal evolution in our experiments will be a key issue in the interpretation. In both ions the absorption spectrum is not drastically dependent on solvent in the polar liquids studied. In polarized absorption experiments on diiodide as a color center in crystals, both transitions were found to be polarized parallel to the molecular axis.[25] Gas-phase potential curves for this molecule have been calculated using experimental data,[26] and are reproduced in Fig. 1 along with the assigned spectroscopic transitions. In Table 1 we present relevant information on triiodide and diiodide along with molecular iodine for comparison. The known gas-phase energetics, and solution thermochemical information on this reaction are summarized in Fig. 2. Using a pump pulse at 308 nm, we find the excess energy in the photolysis to be approximately 1.3 eV into ground-state diiodide, and atomic iodine in the excited spin-orbit state.

Iodine atoms are also formed in the dissociation. Solvated I· in polar solvents is known to absorb weakly in the near UV spectral region[27] (in ethanol, the center of the band is at 400 nm with $\varepsilon = 1400\ M^{-1}\ cm^{-1}$). The charge transfer transition involved, and the decay kinetics which proceed on a nano- to microsecond time scale, have been studied in different solvents.[20,28] Since we will be concentrating on spectral regions outside the range of atomic iodine absorption, and will be observing species with much higher extinction coefficients, the free atoms are not expected to be important in our interpretation.

EXPERIMENTAL

Our laser system is similar to others reported in the literature.[29] Here an outline of the pulse generation scheme is given, with emphasis on novel aspects. A schematic diagram of the apparatus is presented in Fig. 3. The source of femtosecond pulses is an anti-resonant ring synch-pumped dye laser constructed in the lab, and operating at 82 MHz with the Rhodamine 6G / DODCI dye pair. The reflectors surrounding the Rhodamine jet and the DODCI jet are of 10- and 5-cm radii of curvature respectively. The gain dye jet is commercial (Coherent), and that for the saturable absorber homemade, with a pathlength of 10–20 microns. The laser was run with 4 Brewster prisms, without spectral aperturing.

The dye laser is pumped with the frequency-doubled output of an acousto-optically mode-locked and power-stabilized (±1 %) Nd:YLF laser (Quantronix 417) for which we supplied a custom-made RF source as part of an active stabilization scheme for the dye cavity. Synch-pumped femtosecond dye lasers are so stringently dependent upon cavity length that, in

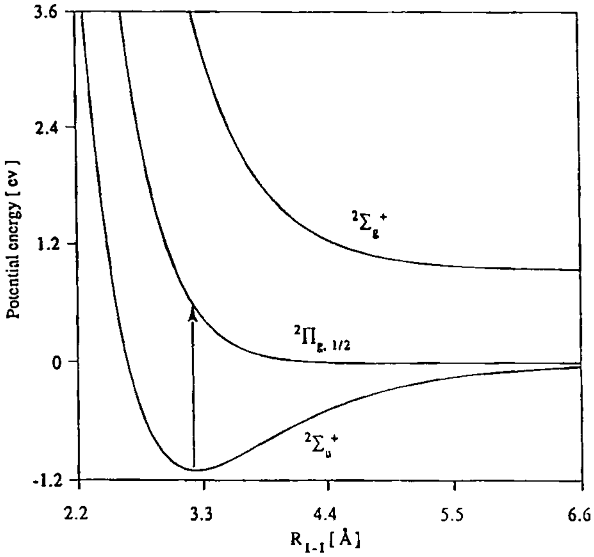

Fig. 1. The gas phase potential curves of the diiodide ion are depicted, including the transition which gives rise to the near IR band studied here. These curves are derived from the work of Chen and Wentworth.[26]

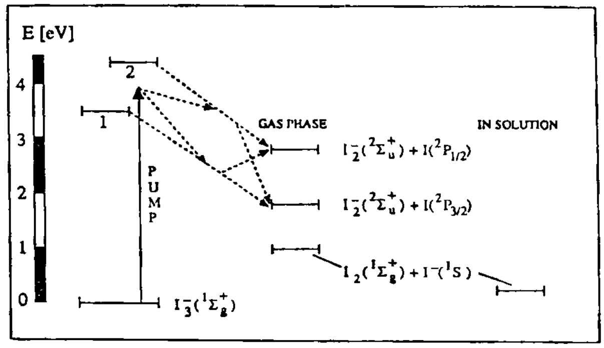

Fig. 2. A schematic energy diagram which includes the origins of ground and excited states of the I_3^- ion, along with those of the relevant asymptotic decomposition channels in the gas phase. The stabilization energy of the lowest decomposition channel by solvation is also included. The pump photon energy used in the experiment is depicted, and the possible processes which may lead from either excited states to the exit channels consistent with our data are included as dashed arrows. The resonance energies for the UV transitions have been taken from solution data.

Table 1. Collection of physicochemical data for tri- and diiodide along with iodine for comparison

	I_3^-	I_2^-	I_2
Equilibrium bond length (Å)	2.9[a]	3.15[b]	2.667[a]
Max absorption concn (M^{-1} cm^{-1})	ε(352) = 2.3*10^4[c] ε(290) = 3.8*10^4	ε(375) = 9400[d] ε(725) = 3500	ε(540) = 900
Vibrational frequencies (cm^{-1})	ν_1 = 111[e] ν_2 = 70 ν_3 = 143	114[f]	214.5[a]
Relative stabilization — gas phase (eV)	to I_2 + I^-: ~1[g] to I_2^- + I: ~1.7	to I + I^-: ~1[f]	to I + I: 1.58[h]
Relative stabilization — in solution (eV)	to I_2 + I^-: ~.25[j]		

(a) Average value in crystals, ref 9b. (b) ref 26. (c) ref 10. (d) ref 24. (e) ref 14b, and Gabes, W.; Gerding, H. *J. Mol. Struct.* 1972, **14**: 267. (f) Tripathi, G.N.R.; Schuler, R.H.; Fessenden, R.W. *Chem. Phys. Lett.* 1985, **113**: 563. (g) ref 18. (h) Huber, K.P.; Herzberg, G. *Constants of Diatomic Molecules*; Van Nostrand Reinhold: New York, 1979. (i) ref 19.

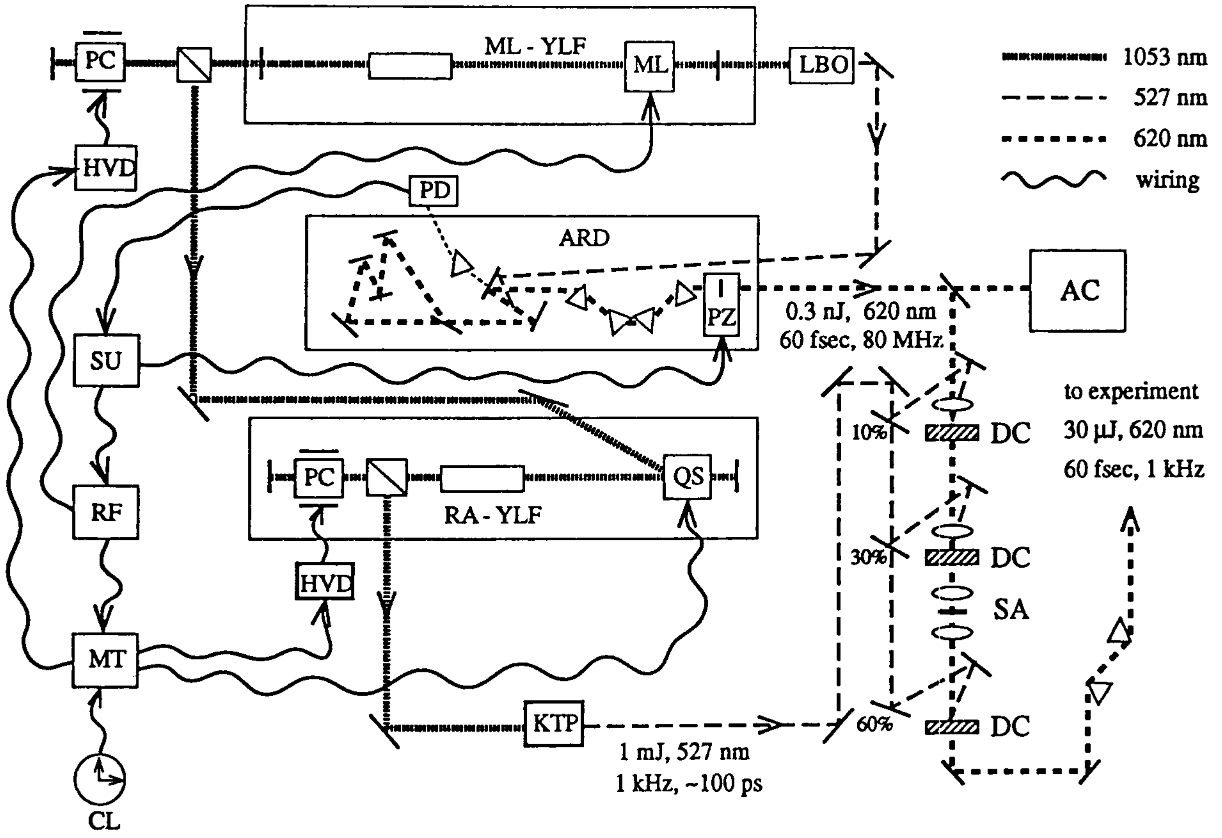

Fig. 3. Schematic diagram of laser setup; ML-YLF — mode-locked Nd:YLF laser, LBO— heated noncritically phase-matched LBO doubling crystal, ARD— anti-resonant ring dye laser, PZ — piezoelectric positioner for output coupler, PD — photodiode, PC — Pockel's cell, HVD — high voltage driver, AC — autocorrelator, QS— Q-switch, RA-YLF — regenerative amplifier, DC — dye cell, SA — saturable absorber, MT — master timer, RF — radio frequency synthesizer, SU — servo unit.

most cases, active stabilization is required both for long- and short-term stability of operation.[30] We have chosen to achieve this by combining the control of the cavity length via a piezoelectric actuator for correcting low frequency 'drift', with slight variations of the RF frequency going to the mode-locker for correcting effective cavity length fluctuations at high frequencies.

The correction signal is generated by dispersing the beam transmitted through a cavity high reflector onto a single PIN photodiode. The difference between the current signal from the photodiode and an adjustable DC current source generates a correction signal which is passed through high- and low-pass filters. The high frequencies are fed into the RF-generating crystal oscillator. This oscillator has a frequency which is DC voltage controlled (Vectron), and its output is used for mode locking. The low-frequency components of the correction signal are amplified in a high-voltage amplifier, and the output fed into the piezoelectric positioner. In this configuration the piezoelectric actuator corrects for perturbations at frequencies from DC up to nearly 1 Hz, and the RF for variations from 1 to 200 Hz. The slight variations in the RF frequency required to stabilize the dye laser (±10 Hz) have no detrimental effects on the YLF laser operation. The typical output of the stabilized dye laser are pulses containing 0.4 nJ of energy with a duration of 60 fs and a central frequency of 615 nm. The described stabilization renders the laser operable continuously with high stability for hours, without recourse to pneumatic isolation of the optical platform.

Amplification of the dye laser pulses is performed in a synchronous 3-stage dye amplifier which is pumped by the doubled output of a Nd:YLF Regenerative Amplifier (RA). The RA is constructed around a commercial CW YLF cavity (Quantronix, 117) prepared for operation as an RA operating at 76 MHz. After adjustment of the cavity length for operation at 82 MHz, acousto-optic (Newport Electro Optics), and electro-optic (Laser Metrics) modulators were added to the amplifier. The electro-optic modulator is configured as a Pockel's cell using a homemade avalanche transistor driver. The single pulse selection and seeding of the RA is performed as previously described. The maximum output of the RA is 3.5-mJ pulses at a repetition rate of 1 kHz, with a peak-to-peak stability of 3–5%. The duration of these light pulses was not directly measured but is expected to be similar to that of the seed pulses, 70–100 ps. In our experiments the output was limited to 1.2 mJ per pulse, and frequency doubled with an efficiency of ~50% in KTP.

The doubled RA pulses are combined collinearly with the dye laser pulses in three amplification stages containing sulfarhodamine 640 in a mixture of water and methanol, producing amplified pulses with an average energy of 25 μJ per pulse, at the repetition rate of 1 kHz. After compensation for group velocity dispersion in a prism pair, the duration of these pulses was identical to that prior to the amplification. Excitation pulses were generated by doubling the fundamental pulses in a 0.5 mm KDP crystal (Quantum Technology), providing 0.5–1 μJ of energy at 308 nm. Cross-correlation times between the doubled and fundamental pulses were measured in an Optical Kerr Effect (OKE) experiment in a thin flow of neat solvent (~200 μm pathlength); typical Kerr cross-correlation times were 100–110 fs long. White light probe pulses were generated in a static cell of D_2O, with 10-nm-wide interference filters for spectral isolation. OKE signals were derived for these pulses also, and produced similar cross-correlation times. These signals were also used to determine zero of relative pump-probe delay. Special care was taken to ensure complete spatial overlap between pump and probe pulses by measuring transmittance of the beams through a small pinhole. The diameter of the probe beam was always smaller than the pump beam spot in the overlap region (typically by about 75%). This procedure is repeated every time the probe wavelength is changed since the size, shape, and focal behavior of the probe beam are wavelength dependent.

A typical problem encountered when using white light segments for probe spectral tunability is that of obtaining reliable relative absorption values at different probe wavelengths. The transient absorption at each wavelength is measured in a separate scan, and varying conditions may cause a substantial error in the relative absorption values. We have minimized this potential error source (where necessary) by taking a few precautions. First of all, experiments were conducted using similar pump intensities and triiodide concentrations. In addition, at the beginning of a new set of transmission scans, absolute transient transmission values at a specific wavelength (620 nm) were measured, and these served to calibrate the relative measurements taken in that set.

Data acquisition was achieved through an SSH module (simultaneous sample and hold, Data Translation) and A/D converter (DAS8-PG, Metrabyte) and processed in a 286 personal computer. The experimental observable is the transient differential transmittance ($\Delta I/Io$), and at each data point the signal was averaged for 50 pulses under the criterion that pump energy falls typically within a ±4% window. The signal was further improved by repetitive scans (in the cleanest scans up to 200 times). I_3^- solutions were prepared by dissolving iodine and KI (best available commercial purity) in ethanol (G.R. or spectroscopic quality, Merck), and concentration determined spectrophotometrically to be ~3 mM. The solution was run through a free-flowing jet, or a quartz flow cell, with an optical path length of 200 μ, in order to prevent temporal response broadening due to the different group velocities of pump and probe pulses.

EXPERIMENTAL RESULTS

Transient transmission data following 308-nm excitation were collected at a series of wavelengths throughout the visible, the near IR, and at the excitation frequency. A full description of all these results can be found elsewhere.[6b] Since our interpretation hinges mainly on our transmission observations in the near IR and red spectral region, and at the wavelength of excitation at 308 nm, we will discuss only these aspects here. The transient changes in transmission in the red portion of the visible and at 308 nm are associated predominantly with the product and reactant ions respectively. We will, accordingly, discuss our results for these spectral regions separately. All preliminary results pertaining to solvents other than ethanol will be stated as such, and all other results will pertain to ethanol solutions only.

Red and Near IR

We primarily focused on this portion of the spectrum since, as pointed out in Spectrochemical Background, at long delay times it is deemed to be dominated by absorption of the product diiodide ions.[24] In the scans in Fig. 4 we present the short time variation of transmission at 2 probe wavelengths following photoexcitation. A sudden

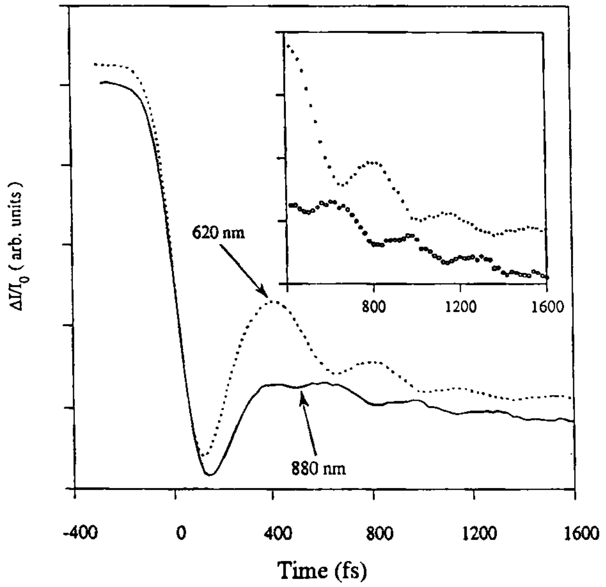

Fig. 4. Transient transmission data at early delay times for two wavelengths situated to the red (880 nm), and to the blue (620 nm), of λ_{max} for the thermally-relaxed near IR band of diiodide (both scans in parallel pump and probe polarization configuration). The inset depicts a portion of the data on an expanded scale to clearly demonstrate the opposed phase of the oscillations in either scan.

rise in absorption is observed throughout the red portion of the spectrum, the duration of which is limited by our system response. At all the probed wavelengths between 880 and 550 nm, this rise is followed by a rapid reduction in absorption which goes on to a delay of nearly 300 fs, giving way to a stage of leveling off or slight increase of absorption. During the latter, weak damped oscillations in the optical density are observed at all probe frequencies. In particular, the phase of these oscillations differs by 1π radians upon changing the probe wavelength from 620 nm (to the blue of λ_{max} [I_2^-]), to 880 nm (to the red of λ_{max} [I_2^-]). This is demonstrated in the inset of Fig. 4 on an expanded scale. At all of the probe wavelengths used in this spectral range the periodic modulations of transmission cannot be traced all the way back to $t = 0$, and appear only after the first rapid fall in OD. A crude process of curve fitting of the oscillations provides a central frequency of 94 ± 5 cm^{-1} and a damping time of 450 ± 50 fs. The agreement with the data is demonstrated in Fig. 5. This qualitative behavior has also been obtained for this reaction in additional solvents such as water (Fig. 6). Even before full quantitative analysis, this demonstrates the generality and reproducability of this observation in a series of polar solvents.

At longer times, the transient transmission data depicted in Fig. 7 exhibit frequency-dependent nearly exponential changes in the absorption, with a time constant of ~4 ps. The variations observed consist of a reduction of absorption in the wings of the band, an increase in absorption at λ_{max}, and constitute an overall narrowing of the 740-nm band.

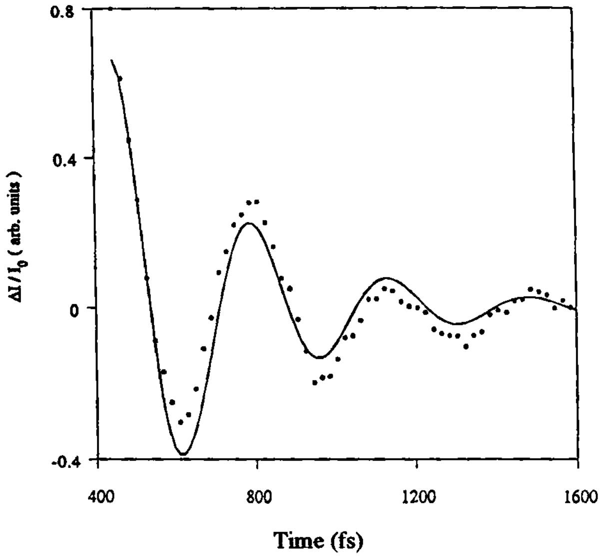

Fig. 5. An approximate fit of the modulations in transient transmission of 620-nm probe pulses by an exponentially decaying harmonic oscillation. See text for details.

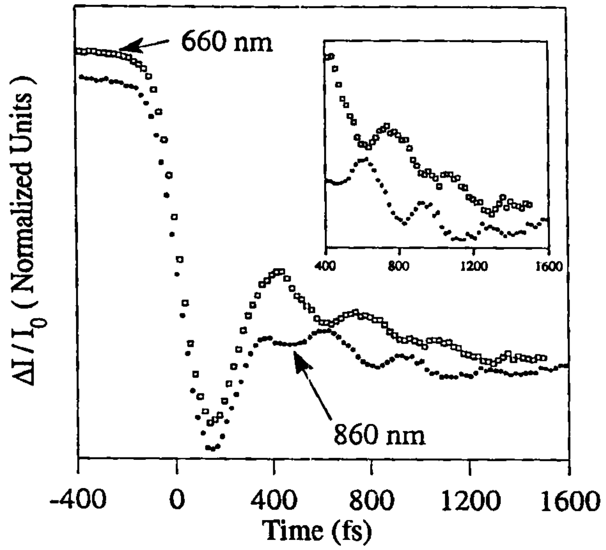

Fig. 6. Same as Fig. 4, for triiodide solution in water.

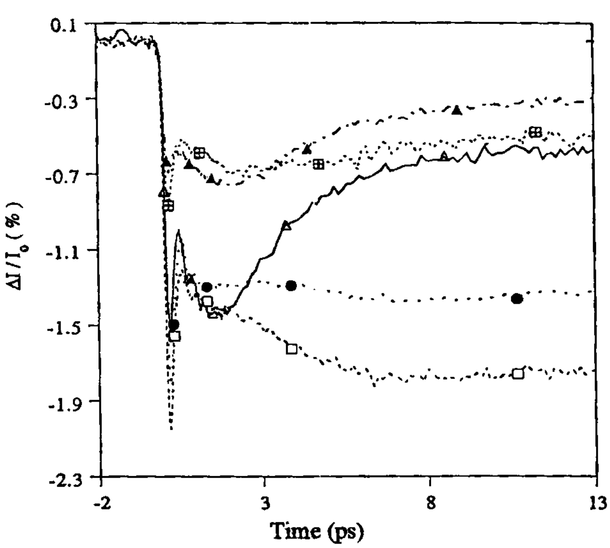

Fig. 7. Long-term transient transmission data as a function of probe delay for a series of wavelengths around, and in the center of, the near IR band of I_2^-. These scans, which were taken at 'magic angle' relative pump and probe polarizations, thus eliminating any reorientational contributions, clearly demonstrate an overall narrowing of the band during the first few picoseconds after dissociation is complete. The error in the relative transmission values at the different wavelengths is estimated to be ~20% (see description in experimental part for details).

Legend:				
	—△—	620 nm	----⊞----	860 nm
	---●---	700 nm	—-▲-—	950 nm
	--□--	760 nm		

As a means of probing the orientational memory of the product ions and the dynamics of their reorientation, a series of photoselective transient transmission scans were run. For identical conditions, the transmission transients were measured once for parallel relative polarizations of pump and probe (VV), and once with perpendicular linear polarizations (VH). Results collected at 620 nm are depicted in Fig. 8 for early and intermediate delay times. The anisotropy plotted is calculated according to eq 2:

$$r(t) = \frac{\Delta I_{VV} - \Delta I_{VH}}{\Delta I_{VV} + 2\Delta I_{VH}} \tag{2}$$

As observed in the figure, the initial value of the anisotropy, ~ +0.2, lies well below the maximum expected value for parallel transitions of 0.4.[31] The anisotropy exhibits two phases of decay: The first is very rapid and is completed within 0.7 ps. The second is fitted to a single exponential with a time constant of 5 ps.

The results reported were checked for artifacts related to two issues: (1) the high intensity of the excitation fields and (2) the relatively high concentration of the triiodide ions in the ethanol solution (~3 mM). In order to check for the former, an intensity dependence of the signal amplitude at various delay times as a function of the excitation pulse energy was followed. At the highest excitation intensities experimented with, a slight nonlinearity was detected, which leads to an accentuation of the initial instantaneous rise in signal, along with some long-term nondecaying absorption background.[32] In the neat solvent we detected a weak absorption signal, the amplitude of which was proportional to the excitation pulse energy squared. Upon addition of iodide ions the same nonlinear signal was observed. We estimate this nonlinearity to contribute no more than 10% to the observed signals for the triiodide samples at the highest pump powers. By reducing the excitation power, a regime was reached where perfectly linear power dependence was observed and all of the salient features reported were manifest in the signal, including the oscillations in the optical density. Wherever possible, we present data collected under such conditions. Only for the finest details of the signal oscillations will we present results outside this regime.

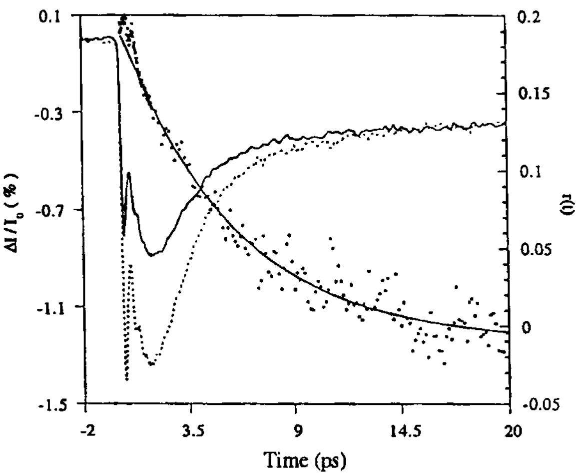

Fig. 8. Transient transmission at 620 for VH (— upper curve), and VV (- - - - lower curve) relative pump and probe polarizations. In the same scan we depict the degree of absorption anisotropy, (··· right Y axis) calculated according to eq 2, and fit to a single exponential from 2 ps delay on (— right Y axis). Possible reasons for the low initial value of $r(0)$ are discussed in the text.

The issue of concentration was investigated to test whether the signal was related to higher aggregates of iodine and iodide, or to ion pairs in the ethanol solvent.[33] This was studied by following the kinetics of transmission probing at 620 nm, after dilution of the solution by a factor of 6. The time-evolution characteristics of the signal were found to be identical at both these concentrations. We therefore conclude that no artifacts related to excessive concentration of the triiodide ions are present.

UV

The time evolution of transmission at the photolyzing wavelength has been recorded in order to follow the process of triiodide recombination.[22,23] This is possible in light of the negligible optical density of diiodide and iodide ions at this wavelength. Unlike the scans we have presented in the visible, where photolysis has induced absorption in an otherwise transparent solution, in the UV we expect to observe an induced bleach or increase of transmission as a result of irradiation at 308 nm. Many of the scans presented pertain to triiodide solutions which are far from being optically thin. We therefore present our results in the form of transient variations in OD.

Figure 9 presents data in the UV at delays of up to 70 ps, utilizing a magic angle polarization combination for the pumping and probing pulses. The insert portrays only the first few ps. An instantaneous bleach, upon which are superimposed rapidly decaying oscillations, which exhibit a period of nearly 300 fs, and a decay time of ~1.5 ps, is observed. Unlike the modulations in transmission observed in the red, these are retraceable all the way to $t = 0$. The distinct nature of the oscillations observed here from those recorded in the visible is exemplified in the Fourier transforms depicted in Fig. 10. The transform derived from the UV data is higher in frequency and narrower than the transform of the 620-nm modulations. The central frequency of the former coincides with the frequency of symmetrical stretch vibrations in the triiodide ions.

At longer delay times the absorption in the UV undergoes replenishment (Fig. 9), and does not take place on a single time scale. In ethanol this replenishment is well characterized by two exponential decays, the first with a characteristic time of 5 ± 1 ps and a contribution of 20%

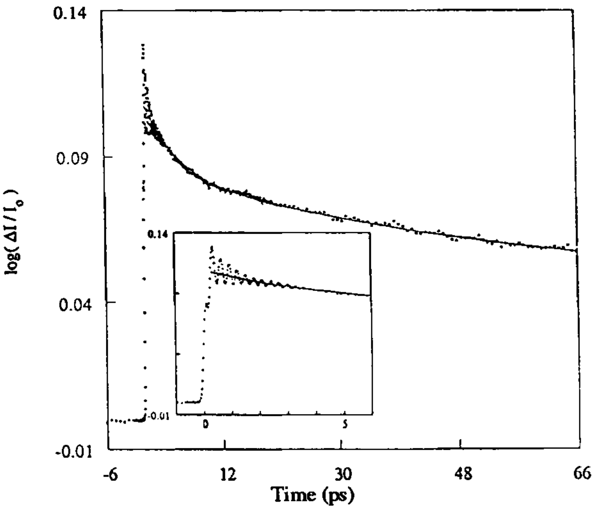

Fig. 9. Magic angle transient bleach scans at the pump wavelength for long probe delays in ethanol solution. Also shown is the best fit to a bi-exponential decay (solid line). The inset expands the initial 5 ps of bleach evolution where strong modulations of the transmission signal are observed.

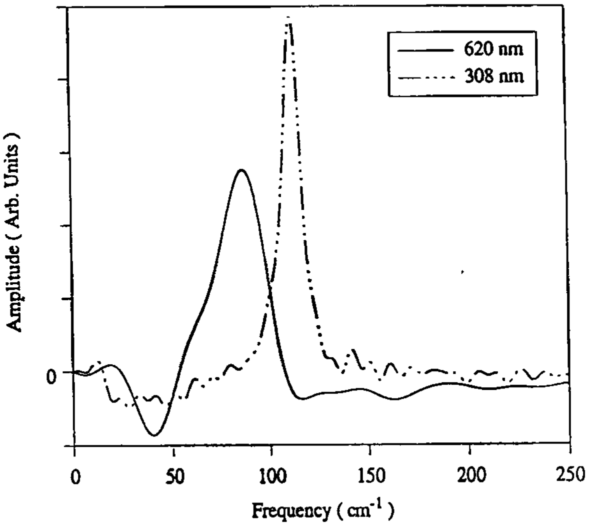

Fig. 10. Fourier transforms of the oscillatory features in the transient transmission data at early times after subtraction of the slower background features. Presented are data from probe frequencies at 620 nm and 308 nm.

to the replenishment, and the second characterized by a time scale of 75 ± 10 ps, and a contribution of ~40 % to the replenishment. With the completion of both these phases of recovery, a residual ~40 % of the bleach is therefore left intact. In order to test the dependence of the replenishment kinetics on the nature of the solvent, a similar scan was run in isobutanol. The results for the bleach kinetics in the UV both for isobutanol and for ethanol are depicted together as transient OD scans in Fig. 11. As in the case of ethanol we can discern two early phases of absorption replenishment, however in the heavier alcohol the initial rapid stage of replenishment is different in appearance, and much more pronounced than in the case of ethanol. It alone corresponds to nearly 50% of a complete rejuvenation of the triiodide OD, and is markedly nonexponential in appearance. The longer portions of transmission changes have not yet been recovered with confidence for isobutanol solution, and this aspect of the signal is currently under study.

Bleach kinetics at 308 nm were studied photoselectively, as in the case of the 620-nm experiments, in order to follow reorientation of the triiodide reactants. The decay of bleach anisotropy at 308 nm for the ethanol solutions is shown in Fig. 12, and fit by an exponential with a time

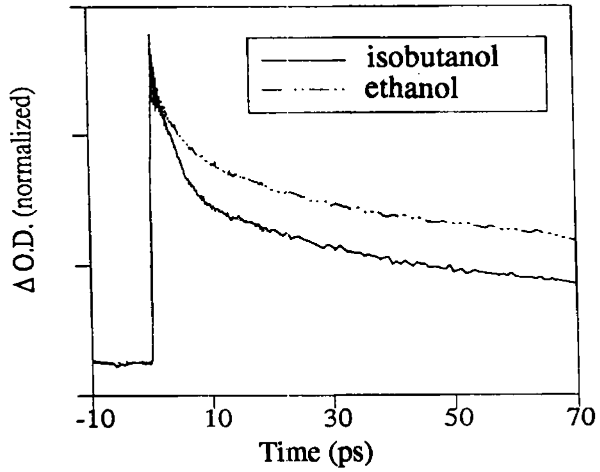

Fig. 11. Transient bleach kinetics at long delays for triiodide solutions in ethanol, and in isobutanol.

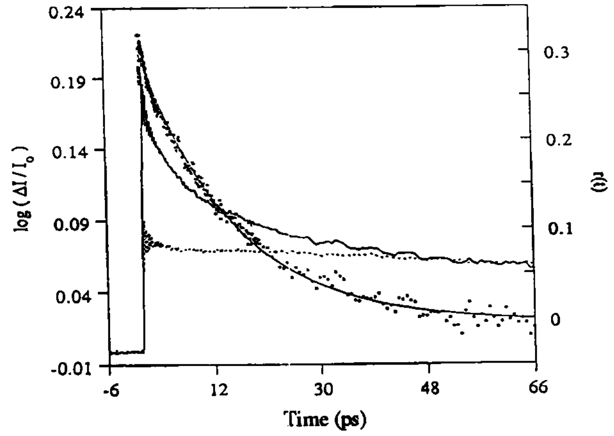

Fig. 12. Transient bleach data in ethanol solution at 308 nm, taken for VV (— upper curve), and VH (- - - lower curve) pump probe relative polarizations. Plotted on the same figure is the anisotropy of the bleach (··· right Y axis), fitted to a single exponential decay of 15 ps (— right Y axis).

constant of 15 ps, decaying 3 times slower than the anisotropy of the photoinduced absorptions in the visible. The initial value of the anisotropy factor is 0.3, substantially higher than the initial value of ~0.2 measured at 620 nm. It is, however, lower than the theoretical limit of 0.4 for pump and probe into a strongly allowed parallel transition. It is likely that this is due to the saturation of the I_3^- absorption in the front portions of the flowing sample.[31]

DISCUSSION

Assignment of Red/Near IR Transients

Sorting out our results must begin with the red and near IR spectral region. This requires first dealing with the instantaneous appearance of absorption over this entire spectral range. From the temporal profile of this rise, and its appearance symmetrically around the independently-determined zero of delay time, we conclude that this absorption must be closely associated with the excited state of I_3^-. It must be stressed that, as pointed out by others,[34] this spectral feature represents a population in transition which has undergone substantial translation during the period of photoexcitation.

The next feature is a rapid stage of reduction in the optical density throughout this spectral region. This portion of the data is assigned to the process of bond fission, and emergence of the nascent fragments. It begins at the peak of the excited-state absorption, near a delay time of ~100 fs, and continues up to a time delay of ~300 fs. In a previous report a simple mechanical model based on the analytical analysis of Bersohn and Zewail[35] was presented for underlining the feasibility of this assignment. In the following section this assignment will be conclusively corroborated by elaborate quantum simulations.

The anisotropy decay is also consistent with assignment of the rapid transmission reduction as the stage of bond fission. At very early times ($t < 1$ ps) overlapping with this stage, a fast component of anisotropy loss is observed (Fig. 8). This may be assigned to rapid loss of orientational memory induced by deposition of excess energy in the fragment rotational motions, and is fully consistent with the much lower initial value of the anisotropy with respect to the value of 0.3 in the case of the 308-nm bleach anisotropy.

We must now deal with the slowly evolving oscillatory phase of signal which follows. This feature must be due to vibronic coherence either in the reactant ions or, conversely, in the fragments. The main considerations that guided our assignment of these oscillations are: (1) The fact that the oscillatory portion of the data has an induction period of nearly half a picosecond in delay time and (2) the fact that these oscillations are at a frequency which is substantially lower than that which characterizes relaxed ground-state vibrations of diiodide ions in solution. These two points preclude a simple RISRS excitation of parent ions, or impulsive direct absorption into a bound state of triiodide, as the mechanisms giving rise to this portion of the data.

The modulation of the optical density must therefore be attributed to a 'product' state. However, an excited state of the parent ion intrinsically bound, or bound by virtue of solvent caging, but which is not directly accessed optically, would also answer this description. We must ascertain whether the oscillations we observe are due to coherent vibration of I_3^- on an electronically-excited surface which is populated through a curve crossing, or of I_2^- fragments which are excited through the process of bond fission.

The photoselective experiments may serve to guide the conclusions concerning this issue. The relaxation of the transmission anisotropy of the red band region decays much faster than that for the bleach at 308 nm, which is clearly a measure of triiodide reorientation in the ground state. This discrepancy points to the fact that the oscillations must be a manifestation of vibronic coherence in a substantially different species.[36] In addition, if the vibrations observed were due to caging of an otherwise dissociative state, it seems unlikely that the vibrations would dephase so slowly or exhibit such high frequencies.[23]

In view of the above considerations, we attribute the oscillations to coherently vibrating nascent I_2^- fragments, produced by direct photodissociation of I_3^-. First and foremost, diiodide ions are expected to exhibit a broad absorption band centered at 740 nm, which is the wavelength of maximal transient absorption observed. This substantially smaller ion could reorient much faster than triiodide, explaining the faster decay of transmission anisotropy.

This assignment is given outstanding support by the opposed phase of the observed oscillations in the transmission of delayed probe pulses at 620 and 880 nm. Due to the bound-to-free nature of the 740-nm absorption band, the resonance frequency is a steep function of the internuclear distance. For a coherent wavepacket whose motion consists of periodic lengthening and shortening of the average internuclear distance, the resonance frequency λ_{max} will accordingly be periodically red- and blue-shifted. At the endpoint of the vibration where the internuclear distance is maximized, the entire spectrum will be shifted to the red. λ_{max} will be shifted closer to the probe pulses at 880 nm and they will suffer enhanced attenuation. In contrast, at this point the absorption maximum has shifted the farthest from 620 nm, and therefore the absorption will be at a minimum. Analogous considerations apply to the other endpoint of vibration. If we accept this picture, then the damping of the modulations must give a time scale for dephasing of this coherence. We will not give a complete account of this aspect here, but as elaborated upon elsewhere, the observed time scale indicates that solvent-induced pure dephasing must be playing a major role in this process.

The fast spectral narrowing of the red diiodide band, which is observed on a 4-ps time scale following the dephasing of the oscillations, is — according to our interpretation — the result of vibrational relaxation of the nascent fragments. It is in general accordance with vibrational relaxation times measured for solvated ions such as azide in water,[37] and for dipolar molecules in polar solvents as derived from simulations.[38] It is also consistent with recent caging and recombination experiments on I_2^- in a series of polar solvents, conducted by Barbara and coworkers.[22] One must also keep in mind that at some of the probed wavelengths, spectral density due to highly vibrationally excited I_3^- could be present.[3]

One would like at this point to say something more quantitative about the nascent I_2^- vibrational distribution. The vibrational distribution of the daughter ions after dephasing should manifest itself in the shape of the absorption band. In order to gain an elementary appreciation of the nascent diiodide vibrational distribution, we present calculated absorption spectra of various dephased vibrational populations, to compare with the transmission data.

The absorption cross section, σ_A, for the diiodide eigenstates as initial states, was calculated by Heller's time-dependent formalism according to eq 3:[39]

$$\sigma_A(E_L) \propto \mu^2_{i\rightarrow f} \int_{-\infty}^{\infty} \langle \phi(0)|\phi(t)\rangle \exp[i(E_L + e_i)t/h]dt \quad (3)$$

E_L is the laser photon energy, e_i the vibrational energy of the initial state $\phi(0)$, and $\phi(t)$ is this initial wavefunction propagated after instantaneous promotion at $t = 0$ on the excited potential. In the calculation we used quantum mechanical time domain propagation techniques. The eigenstates for ground-state diiodide were calculated using the potential in Fig. 1 by the relaxation method.[40] Following this, the wavepackets were propagated on the excited state by using the Chebychev propagation scheme.[41] The correlation functions calculated were transformed according to eq 3 to obtain the spectrum. The spectra of different incoherent distributions is then calculated by a weighted superposition of these results. We again stress that in these calculations the diiodide gas-phase potential curves were used, slightly shifted in energy in order to obtain agreement with the resonance frequency, and only the red absorption band was considered.

In Fig. 13 we depict two absorption spectra, one of a thermal room temperature distribution, and the other of a dephased Gaussian population, 800 cm^{-1} wide (fwhm), and centered at $v = 17$ (assuming a constant dipole moment). This vibrational level is characterized by a frequency near that detected in our experiments. We see that after dephasing, a narrowly distributed population centered at $v = 17$ absorbs quite widely, ranging from 0.55 to 1.3 microns, and has a double-humped appearance, devoid of a central maximum at 740 nm. These results demonstrate vividly that cooling will cause a narrowing of the near IR absorption band, as we in fact observe in our experiments (Fig. 7). However, the sparse spectrum to be obtained from our data lies qualitatively between the two extremes depicted in the calculated spectra. It is possible that a much broader distribution of vibrational levels is produced through the photolysis, including low vibrational levels, giving rise to the high absorption at the central frequency.

Molecular dynamics simulations are underway to gain quantitative information concerning the vibronic distribution generated by photolysis, and a preliminary communication has been published.[42] In these simulations rapid solvent-induced relaxation of all forms of fragment energy is found, and the calculations serve to demonstrate the central role played by the solvent in molding the vibronic state of the fragments. It is instructive to relate these results to the behavior expected of an isolated ion given the same model of intermolecular forces both in the ground and excited states. Quantum mechanical simulations conducted for this purpose will be presented in the next section.

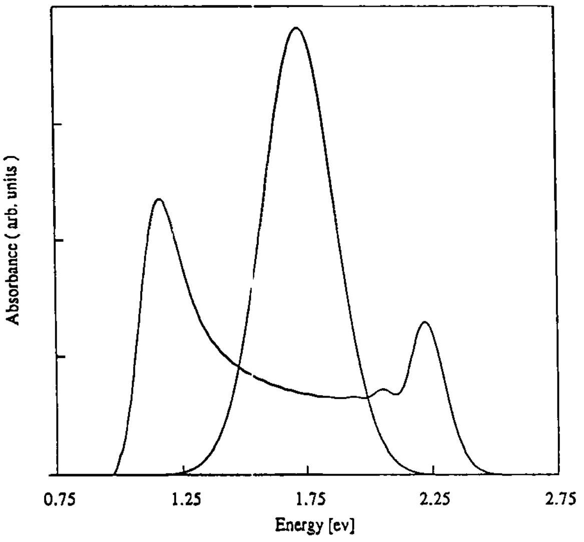

Fig. 13. Simulated absorption spectra associated with the near IR band of I_2^-, for two vibrational population distributions: a room temperature thermal distribution, and a 800 cm^{-1} Gaussian distribution, centered at $v = 17$. See text for details.

UV Transients

The transition to oscillations at 110 cm^{-1} in the near UV data must be associated with the Resonance Impulsive Stimulated Raman Scattering (RISRS) excitation of the symmetric stretching mode of the triiodide ground state.[1a–h] The impulsive nature of the excitation process allows the burning of a 'coherent hole' in the ground-state triiodide eigenstates, creating an oscillating linear combination of states that subsequently evolves periodically at the stretching frequency. This modulation is manifest in all of our near UV probing experiments, and according to the described nature of this process, the spectral modulations produced are retraceable back to the zero of delay time. We would like to emphasize the point that in the sample there are *two different chemical species which vibrate coherently*, the nascent diiodide fragments, and the triiodide remaining on the ground electronic state, due to different excitation mechanisms. We note here, in passing, that we found the relative depth of our RISRS modulation in the UV to be dependent on the pump power. We defer analysis of this result to a later publication that will deal with this process explicitly.

Aside from this manifestation of the impulsive nature of our photoexcitation stage, the UV transients contain information concerning geminate recombination. The fast component of UV absorption replenishment may be associated with geminate recombination of I_3^-, followed by vibrational relaxation on its ground state. The time scale of this combined process is consistent with the accumulating data on rates of primary geminate recombination in iodine, and with vibrational relaxation times of ionic species in polar solvents.

Before discussing the pathways of recombination, we must establish the limiting quantum yield for diiodide production. Concentrating on our results for ethanol for the purpose of this exercise, this value is calculated at ~10 ps of delay. At this delay the very rapid signal variations have subsided, and vibrational relaxation in the diiodide is complete. By comparing the ratio $(\Delta OD_{740}/\varepsilon[I_2^-]_{740\,nm})$ to $(\Delta OD_{308\,nm}/\varepsilon[I_3^-]_{308\,nm})$, using the published extinction coefficients of di- and triiodide ions,[10,24] we find that within experimental error, nearly 100% of the unrecombined triiodide has dissociated to produce diiodide fragments. In order to further test the plausibility that I_3^- replenishment may proceed via the reverse of eq 1 at long delay times, we have compared the long time decay kinetics of triiodide OD with normalized absorption decays at wavelengths associated with the red I_2^- band. This is depicted in Fig. 14. It is seen that within our experimental error, the normalized decay kinetics are identical. This demonstrates that replenishment of triiodide absorption from 10 ps onward is solely achieved through the geminate recombination of diiodide and iodine atoms, and that from this delay time diiodide fragments make up for 100% of the dissociated I_3^-. At later delays diffusion-controlled processes of diiodide formation and disproportionation occur, but these stages are not observed here.

We are relying here on transmission data at a single wavelength to characterize the changes in triiodide concentrations. Such an approach led to erroneous conclusions in early ultrafast work on iodine recombination dynamics, due to the fact that the rate-determining step for absorption replenishment was vibronic and not electronic relaxation. This complication is alleviated here for the long recombination components, due to the rapid rate of vibrational relaxation in the ionic species we are probing.

Given our lack of detailed information concerning the topology of triiodide potential surfaces, specific mechanisms for recombination in the triiodide case cannot be given at this stage. The simplest scenario is that the rapid decay component at 308 nm is due to primary recoupling of the fragments directly from diiodide and iodine atoms, followed by vibrational relaxation. This would require the ground state to correlate to these fragments, or low-lying curve crossings which facilitate the recombination. The remaining population has separated and recombines more slowly.

Within this conceptual framework, it is interesting to compare the results of UV transients recorded for solu-

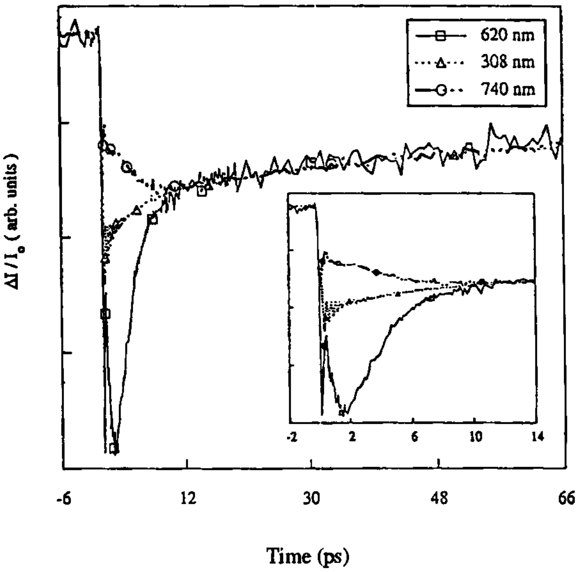

Fig. 14. Transient transmission data (magic angle configuration) for two wavelengths within the near IR diiodide band, and inverse transient changes of log transmission at the pump frequency. The data scans were normalized in order to demonstrate the identical kinetic behavior from ~10 ps onwards. In the inset, an enlargement of the initial features is shown.

tions in the two alcohols reported. The main conclusion is that the heavier solvent is more effective in caging the dissociation fragments and inducing primary geminate recombination. This result is particularly interesting in light of the fact that the increase in the mass of the alcohol molecules is accompanied by a reduction in the polarity of the solvent. It seems that for the homologous series of alcohols, the solvent mass, and not its long-range attractive interaction with the solute, determines the caging efficiency. This is in agreement with the recombination experiments of diiodide ions in similar solvents.[22] A full study of solvent dependence is being conducted and will shortly be reported.

PHOTODISSOCIATION CALCULATIONS

Starting quantitative analysis of our results requires a simplified model describing the I_3^- ground and excited potential energy surfaces, and the nonadiabatic coupling between these surfaces. These potential surfaces are a function of the I_3^- coordinates, stretches and bends, and all solvent degrees of freedom. Ab initio potential energy surfaces for the full system are extremely difficult to calculate due to the large number of valence electrons and the large spin orbit coupling in iodine. The result of this complicated electronic structure is reflected in the overlapping absorption bands of I_3^-. The complicated electronic structure of I_3^- is also reflected in the electronic structure of the photodissociation product I_2^-, where a multitude of excited states has been calculated, even leaving out the influence of the solution.

The simulation of the dynamics of this system can be approached either classically or quantum mechanically. Due to the heavy masses of the photodissociating fragments involved, it is tempting to assume that quantum effects are minor and to use classical mechanics. This approach is explored by Benjamin et al.[42] who have constructed a full molecular dynamics simulation on the same potential energy surface, including the solvent. The main results of the classical simulations are that both the vibrational and translational excess energies are relaxed on picosecond time scales, and that the coherent vibration of the fragment ions is observable through the absorption probing scheme employed in the experiment, in spite of the very strong coupling of the products and the solvent.

In this paper we want to explore a quantum approach. The heavy masses involved mean very large momenta whose quantum calculations are extremely time-consuming. Nevertheless quantum effects are manifest, in particular in the large dispersion the wave function exhibits in the dynamics. The choice of a quantum simulation stems also from our intention in the future to include a full simulation of radiative coupling of the ground and excited potentials with intense laser pulses. Before actual calculations can take place, a drastic reduction in the complexity of the system is required. The first assumption is that the iodine degrees of freedom are kinetically separated from the solvent. This is probably true only for very short times. But this assumption will be used throughout the calculation. A long time description has to include dephasing and dissipation caused by the solvent. This requires the solution of the Liouville–von Neumann equation, a project which will be reported separately. A second assumption is to consider a collinear model of I_3^- This is justified since the ground state of I_3^- is collinear and no bending overtones are observed in the RR spectrum. The third and most drastic assumption is collapsing all the excited state potentials into one representative potential energy surface.

This potential was fitted to a LEPS functional form, adjusted to an I_2^- asymptotic channel producing an iodine fragment in the ($^2P_{1/2}$) state. The vertical transition from the ground state was adjusted to the blue band of the I_3^- absorption spectrum, and the slope of the potential in the symmetric stretch direction was adjusted semiclassically to give an absorption width comparable to that of the experimental spectrum for a room temperature dephased population. The potential parameters are shown in Table 2. It should be noted that the vertical transition point has an excess energy of ~0.4 eV above the three-body dissociation limit. The photodissociation process was simulated on the assumption of a weak, coherent, and infinitely short excitation pulse. Strong pulse effects can also be simulated and are currently being investigated. Using a formulation originated by Gordon and Heller, the process is simulated by placing the ground surface wave function on the excited potential. The weak field absorption spectrum is obtained by the Fourier transform of the autocorrelation function. The final state distribution is obtained by energetically analyzing the asymptotic wavefunction for the I_3^- system and harmonic ground-state potential was used for the symmetric and antisymmetric stretch modes.

The harmonic ground surface potential leads to a Gaussian ground-state wave function (the parameters are shown in Table 2). The propagation on the excited surface was carried out on a grid by the Chebychev method, using the Fourier scheme for evaluating the Hamiltonian operator.[41] The parameters of the grid and simulation time steps are summarized in Table 2. Figure 15 shows snapshots of the wave function at different times after the initial packet was placed on the excited surface. The initial motion is along the symmetric stretch. The striking feature is a large dispersion along the antisymmetric stretch exhibited by the wave function, which is approximately 2 Å after 200 fs. This dispersion eventually leads the wave function into the asymptotic channels with negligible amplitude

Table 2. Parameters for the I_3^- potential surfaces, and control parameters for the simulations

Ground state potential for I_3^-		
$r^{eq}_{(I-I)} = 2.97$ Å	$\omega_{SYM.} = 110\ cm^{-1}$	$\omega_{ASYM.} = 149\ cm^{-1}$
Excited state potential for I_3^-; (LEPS potential)		
$^1r^{eq} = 3.23$ Å	$^3r^{eq} = 2.983$ Å	
$^1\beta = 1.16$ Å^{-1}	$^3\beta = 1.00$ Å^{-1}	
$^1D = 1.1$ eV	$^3D = 1.009$ eV	
Control parameters for simulation		
$\Delta x = \Delta y = 0.01739$ au		
Dimensions of grid = 1024 × 1024		
Basic time step, $\Delta t = 1000$ au		
Order of Chebychev polynomials, 238		

into the three-body dissociation channel, although this channel is energetically allowed. Even before a detailed evaluation of these results begins, our conclusions concerning the assignment of the first ~300 fs to the initial act of bond fission gain support. We see that the first 12,000 au go by before substantial 'filling' of the asymptotic exit channels begins.

From the two-dimensional plots of the wavepacket at various delay times, it appears that at delays of $t = 14{,}000$ au and onward (Figs. 15d–f), ψ is dispersed quite evenly over all accessible internuclear distances of the diatomic fragment. At the longest delay time of 20,000 (~0.5 ps), at different points along the exit channel, there is bunching up of the packet both at short and long I_2^- radii, and a continued influx of population from the direction of the three-body dissociation rift. In order to make sense of this complex wavefunction we have reduced the wave packet in one dimension, and produced a histogram of $P(R)$, the probability for fragment diiodide ions to be distanced by internuclear radius R, at various delay times. This series of histograms is shown in Fig. 16. We see that in spite of the fact that 'late comers', or those portions of the wave function that enter the dissociation channel after $t = 16{,}000$, are still entering the channel throughout the delays studied, the influx is steadily reduced. The portion of dissociating systems which entered directly at early times has already experienced an intramolecular 'collision', and reextended to the large radius turning point of the motion. This point in the evolution of the system corresponds to a delay for which the classical simulations demonstrate a maximum in the 'red' absorption at 880 nm.

In order to evaluate the distribution of vibrational energies in the fragment ions within the exit channel, the portion of the wave packet described in Fig. 16 was resolved into eigenstates at two delays — at 14,000 and 20,000 au. These distributions are depicted in Fig. 17. We see that the population of fragment ions produced directly at early times produces a very wide distribution maximized at rather high quanta of $\sim v = 40$. The 'late-comers' make a completely different contribution to the distribution which is very localized in vibronic eigenspace, with an acute maximum above $v = 42$. In either case the average portion of excess energy into vibration agrees very well with the prediction of 25% derived from kinematic considerations alone.

To begin with, the excess vibrational energy deposited in the diiodide fragment is much higher than is expected by any of the criteria we have previously discussed, such as the frequency of the coherence or the breadth of the absorption spectrum. This is not surprising since we have not included the influence of the solvent. It is, however, tempting to speculate how the seemingly distinct two populations, the 'early- and late-comers' should fare upon encounter with the solvation layer, and vis-a-vis the preparation of coherence in diiodide fragments. The MD simulations of this and of previous systems demonstrate that by far the most rapidly dephased and dissipated motion in solution will be fragment translation.[7,42] The population which decides early on which pair of iodine nuclei will be diiodide, will from that point on vibrationally evolve relatively independently of the solvent, and aside from the question of recombination via curve crossing, which is not addressed here, the translations will be of little consequence thereafter. These early-comers will therefore behave similarly if not identically in gas phase and solution with respect to vibrational coherence.

The late-comers, in contrast, continue to evolve as if all intramolecular motion were translation. This should lead to a total crash of the system into the solvent shell, leading to extensive energy transfer and dephasing of this portion of the wave function, which in our isolated ion model forays deep into the region of three-atom separation, before settling into a two-body dissociation. For this reason we believe that upon solvation any coherence in vibration must be due predominantly to the early-formed diiodide ions, and the more delayed dissociation should produce relatively cold and dephased fragments.

This expectation is borne out partially by the MD simulations discussed,[42] but here we have only considered the role played by the solvents' strong repulsive interaction. The static and dynamic effects of the attractive polar interactions could also strongly influence the stage of charge rearrangement which accompanies the entrance of the reaction channel.[43] The stabilization of the newly-formed and negatively-charged diiodide by strongly polar solvents could effectively 'sharpen' the wedge dividing the two exit routes, thus enhancing the

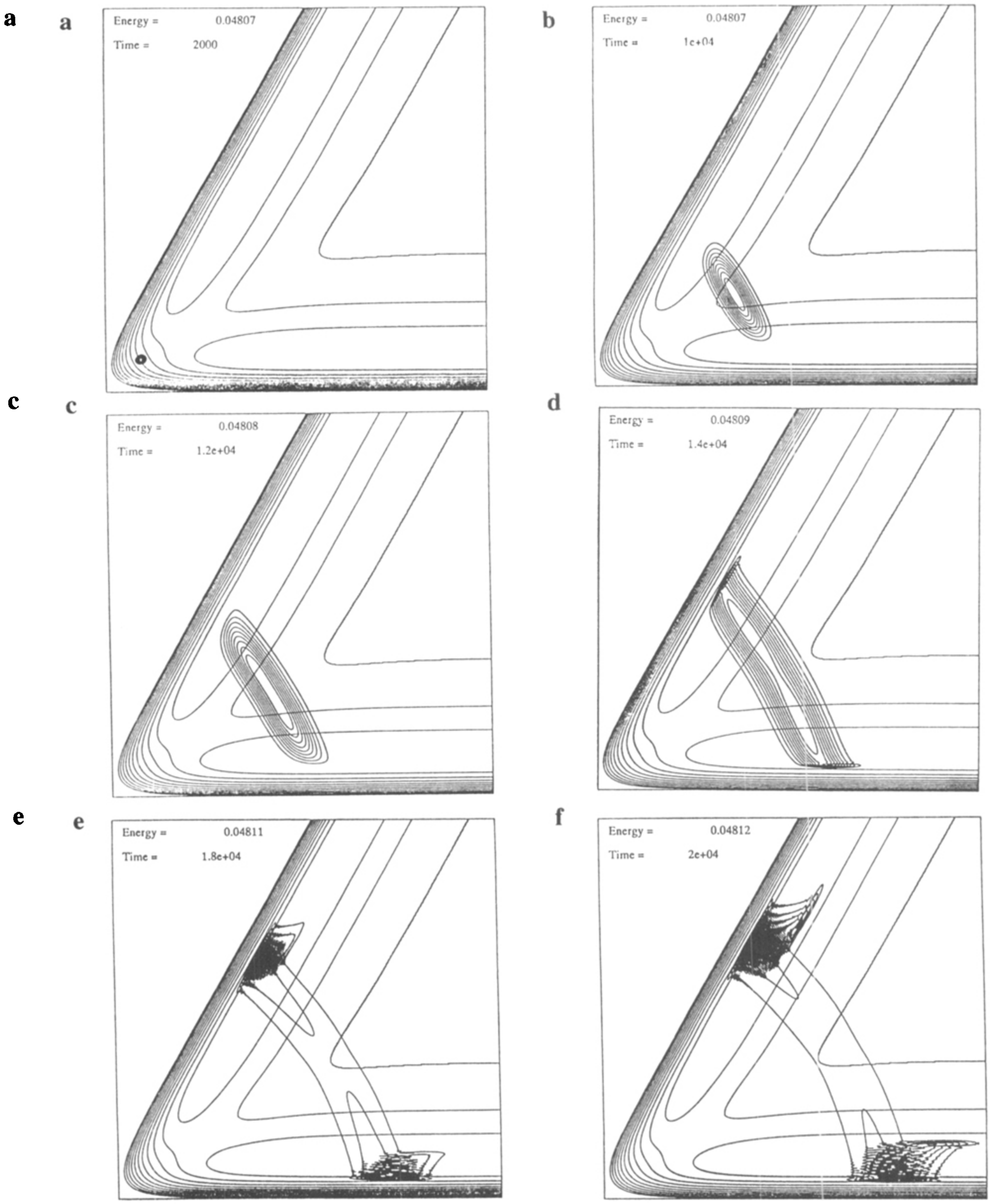

Fig. 15. A series of snapshots of the evolving wave packet following instantaneous photoexcitation at $t = 0$. The wave function is depicted as contours connecting points where $|\psi^2|$ has equal values. The division of the function into contours is normalized to the peak value of $|\psi^2|$, and along with the wave function we have also depicted equipotential contours of the reactive LEPS potential. The time delay is given for each snapshot in au.

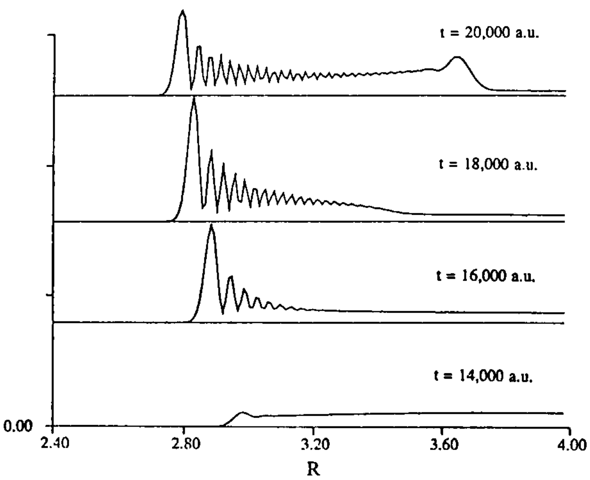

Fig. 16. An overlay of histograms depicting the probability of nascent diiodide fragments to be at a certain internuclear distance, within the asymptotic exit channel. Histograms are given for four delay times designated in the figure.

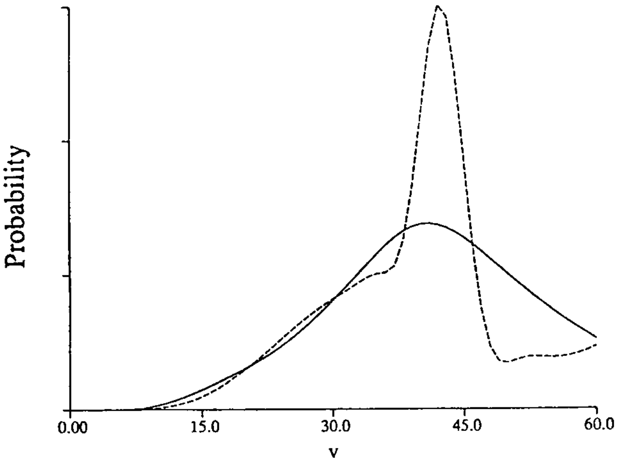

Fig. 17. A resolution into eigenstates of the portion of the wave function which has reached the exit channel at two delay times, 14,000 (solid line) and 20,000 (dashed line) au. See text for details.

early choice of the diiodide fragment, and enhancing the coherence in the nascent fragment distribution. Finally, when judging our simulation results it is important to remember that the very wide initial energy distribution which is generated in the triiodide by the 'instantaneous' excitation may strongly exaggerate the degree of dispersion experienced by the reactive wave packet. A continued effort to combine both the quantum and classical approaches, including attention to the real finite durations of our pulses, and variation of the surrounding solvent, is underway to answer these and many other fundamental questions concerning dynamics of this reaction in solution.

CONCLUSION

In this paper we have reported femtosecond time-resolved transient transmission experiments following photolysis of triiodide ions in polar solvents. Through our experiments we have been able to characterize the time scales for coherent evolution and relaxation of all diiodide fragment motions. By probing the evolution of transmission in the parent ion absorption band, we demonstrated that impulsive photoexcitation leads to a strong coherent vibration of the triiodide ions left in the ground state. A fast component in the bleach decay which is assigned to primary recombination followed by vibrational relaxation of ground-state triiodide ions is found to appear more strongly in the recombination of photolyzed triiodide in heavy alcohols. As a first stage in quantitative analysis of this reaction, we introduced a simplified model for the reactive potential surface. Quantum simulations on this surface support our tentative assignment for the spectroscopic signature of the stage of bond fission. They have raised intriguing elementary questions concerning .the flow of energy during this reaction, and serve as a zero-order approximation of the dissociation in solution.

An especially noteworthy result that we wish to stress is the demonstration of nuclear phase coherence conservation throughout the stage of bond fission to the separated dissociation fragments. This coherence stems directly from the act of impulsive photoexcitation which selects a well-defined coherent superposition in reactant phase space, and is observable exclusively in the time domain. Scrutiny of the amplitude and phase of the coherent product vibration may provide important new information concerning the reactive potential surfaces and interaction with the solvent. A preliminary report of classical simulations of triiodide dissociation indicates that this is in fact the case.[42]

Acknowledgments. We thank A. Waldman and Dr. E. Mastov for technical assistance, and Prof. I. Benjamin for opening our eyes to the complexity of the solvation effects through the MD simulations. This work was supported by the Israel Science Foundation of the Israel Academy of Sciences and Humanities, and by the James Frank Binational German–Israel Programme in Laser–Matter Interaction. The Farkas and the Fritz Haber Centers are supported by the Bundesministerium fur die Forschung, and the Minerva Gesellschaft fur die Forschung.

REFERENCES

(1) (a)Yan, Y-X.; Gamble Jr., E.B.; Nelson, K.A. *J. Chem. Phys.* 1985, **83**: 5391. (b) Walmsley, I.A.; Wise, F.W.; Tang, C.L. *Chem. Phys. Lett.* 1989, **154**: 315. (c) Chesnoy, J.; Mokhtari, A. *Phys. Rev. A* 1988, **38**: 3566. (d) Mukamel, S. *Ann. Rev. Phys. Chem.* 1990, **41**: 15. (e) Walsh, A.M.; Loring, R.F. *Chem. Phys. Lett.* 1989, **160**: 299. (f) Hartke, B.; Kosloff, R.; Ruhman, S. *Chem. Phys. Lett.*

1988, **158**: 238. (g) Ruhman, S.; Kosloff, R. *J. Opt. Soc. Am. B.* 1990, **7**: 1748. (h) Dexheimer, S.L.; Wang, Q.; Peteanu, L.A.; Pollard, W.T.; Mathies, R.A.; Shank, C.V. *Chem. Phys. Lett.* 1992, **188**: 61. (i) Baumer, T; Engel, V.; Rottgermann, C.; Strunz, W.T.; Gerber, G. *Chem. Phys. Lett.* 1992, **191**: 639. (j) Scherer. N.F.; Carlson, R.J.; Matro, A.; Du, M.; Ruggiero, A.J. Romero-Rochin, V.; Cina, J.A.; Fleming, G.R.; Rice, S.A. *J. Chem. Phys.* 1991, **95**: 1487. (k) Ruhman, S.; Joly, A.G.; Nelson, K.A. *IEEE J. Quant. Electr.* 1988, **QE24**: 460. (l) Rosker, M.J.; Dantus, M.; Zewail, A.H. *J. Chem. Phys.* 1988, **89**: 6113. (m) Rosker, M.J.; Dantus, M.; Zewail, A.H. *J. Chem. Phys.* 1988, **89**: 6128. (n) Zewail, A.H. *Faraday Discuss. Chem. Soc.* 1991, **91**: 207.

(2) Myers, A.B. *J. Opt. Soc. Am. B.* 1990, **7**: 1665.

(3) Harris, A.L.; Brown, J.K.; Harris, C.B. *Ann. Rev. Phys. Chem.* 1988, **39**: 341 and references therein.

(4) (a) Xu, X.; Yu, S-C.; Lingle, R.; Zhu, H.; Hopkins, J.B. *J. Chem. Phys.* 1991, **95**: 2445; ibid 1990, **93**: 5667. (b) Paige, M.E.; Harris, C.B. *Chem. Phys.* 1990, **149**: 37. (c) Smith, D.E.; Harris, C.B. *J. Chem. Phys.* 1992, **96**: 5544.

(6) (a) Banin, U.; Waldman, A.; Ruhman, S. *J. Chem. Phys.* 1991, **95**: 2445. (b) Banin, U.; Ruhman, S. *J. Chem. Phys.* 1993, in press.

(7) Benjamin, I.; Wilson, K.R. *J. Chem. Phys.* 1989, **90**: 4176.

(8) Dantus, M.; Bowman, R.M.; Gruebele, M.; Zewail, A.H. *J. Chem. Phys.* 1989, **91**: 7437.

(9) (a) Popov, A.I. In *Main Group Elements Group 7 and Noble Gases*; V. Gutman, Ed., Inorganic Chemistry ser. 1 vol. 3, ch. 2, Butterworths 1972. (b) Downs, A.J.; Adams, C.J. In *Comprehensive Inorganic Chemistry*; Bailar, Jr. J.C.; Emelus, H.J.; Nyholm, R.; Trotman-Dickenson, A.E., Eds., Pergamon Press: Oxford 1973; Vol. 2, 1534.

(10) (a) Gabes, W.; Stufkens, D.J. *Spectrochim. Acta, Part A*, 1974, **30**: 1835. (b) Mizuno, M.; Tanaka, J.; Harada, I. *J. Phys. Chem.* 1981, **85**: 1789. (c) Okada, T.; Hata, *J. Mol. Phys.* 1981, **43**: 1151.

(11) Isci, H.; Mason, W.R. *Inorg. Chem.* 1985, **24**: 271.

(12) Roy, J.C.; Hamill, W.H.; Williams, R.R., Jr. *J. Am. Chem. Soc.* 1955, *77*: 2953.

(13) (a) Barkatt, A.; Ottolenghi, M. Mol. Photochem. 1974, **6**: 253. (b) Fournier de Violet, P; Bonneau, R.; Joussot-Dubien, J. *Chem. Phys. Lett.* 1974, **28**: 569.

(14) (a) Kaya, K.; Mikami, N.; Ito, M. *Chem. Phys. Lett.* 1972, **16**: 151. (b) Keifer, W.; Bernstein, H.J. *Chem. Phys. Lett.* 1972, **16**: 5.

(15) Mohammad, M.R.; Sherman, W.F. J. Mol. Struct. 1984, **27**: 115.

(16) (a) Pimentel, G.C. *J. Chem. Phys.* 1951, **19**: 446. (b) Datta, S.N.; Ewig, C.S.; Van Wazer, J.R. *J. Mol. Struct.* 1978, **48**: 407. (c) Novoa, J.J.; Mota, F.; Alvarez, S. *J. Phys. Chem.* 1988, **92**: 6561. (d) Sæthre, L.J.; Gropen, O.; Sletten, J. *Acta Chem. Scand.* 1988, **A42**: 16.

(17) Tasker, P.W. *Mol. Phys.* 1977, **33**: 511.

(18) Topol, L.E. *Inorg. Chem.* 1971, **10**: 736.

(19) Palmer, D.A.; Ramette, R.W.; Mesmer, R.E. *J. Solution Chem.* 1984, **13**: 673.

(20) Fornier de Violet, Ph. *Rev. of Chem. Inter.* 1981, **4**: 122 and references therein.

(21) Okada, T. *J. Phys. Soc. Jpn.* 1981, **50**: 582.

(22) Johnson, A.E.; Levinger, N.W.; Barbara, P.F. *J. Phys. Chem.* 1992, **96**: 77841. Kliner, D.A.V.; Alfano, J.C.; Barbara, P.F. *J. Chem. Phys.* 1993, **98**: 5375.

(23) (a) Papanikolas, J.M.; Gord, J.R.; Levinger, N.E.; Ray, D.; Vorsa, V.; Lineberger, W.C. *J. Phys. Chem.* 1991, **95**: 8028. (b) Papanikolas, J.M.; Vorsa, V.; Nadal, M.E.; Campagnola, P.J.; Gord, J.R.; Lineberger, W.C. *J. Chem. Phys.* 1992, **97**: 7002.

(24) (a) Dobson, G.; Grossweiner, L.I. *Rad. Res.* 1964, **23**: 290. (b) Fornier de Violet, Ph.; Bonneau, R.; Joussot-Dubien, J. *Chem. Phys. Lett.* 1974, **28**: 569. (c) Baxendale, J.H.; Sharpe, P.; Ward, M.D. *Int. J. Radiat. Phys. Chem.* 1975, **7**: 587.

(25) Delbecq, C.J.; Hayes, W.; Yuster, P.H. *Phys. Rev.* 1961, **121**: 1043.

(26) Chen, E.C.M.; Wentworth, W.E. *J. Phys. Chem.* 1985, **89**: 4099.

(27) de Violet, Ph.; Bonneau, R.; Joussot-Dubien, J. *Chem. Phys. Lett.* 1973, **1**: 251.

(28) Treinin, A.; Hayon, E. *Int. J. Radiat. Phys. Chem.* 1975, **7**: 387.

(29) Ruhman, S.; Kohler, B.; Joly, A.G.; Nelson, K.A. *IEEE J. Quant. Wlectr.* 1988, **QE24**: 470.

(30) (a) Chesnoi, J.; Fini, L. *Opt. Lett.* 1986, **11**: 635. (b) Dawson, m.D.; Maxson, D.; Bogges, T.f.; Smirl, A.L. *Opt. Lett.* 1988, **13**: 126.

(31) Albrecht, A.C. In *Progress in Reaction Kinetics*; Porter, G., Ed.; Pergamon Press: 1970; Vol. 5.

(32) Joly, A.G.; Nelson, K.A. *Chem. Phys.* 1991, **152**: 69.

(33) Milne, J. *Spectrochim. Acta* 1992, **48A**: 533.

(34) Williams, S.O.; Imre, D.G. *J. Phys. Chem.* 1988, **92**: 6648.

(35) Bersohn, R.; Zewail, A.H. *Ber. Bunsenges. Phys. Chem.* 1988, **92**: 373.

(36) Alavi, D.S.; Hartman, R.S.; Waldeck, D.H. *J. Chem. Phys.* 1990, **92**: 4055.

(37) Owrutsky, J.C.; Kim, Y.R.; Li, M.; Sarisky, M.J.; Hochstrasser, R.M. *Chem. Phys. Lett.* 1991, **184**: 368.

(38) Whitnell, R.M.; Wilson, K.R.; Hynes, J.T. *J. Chem. Phys.* 1990, **94**: 8625; ibid 1992, **96**: 5354.

(39) Heller, E.J.; Sundber, R.L.; Tannor, D. *J. Phys. Chem.* 1982, **86**: 1822.

(40) Kosloff, R.; Tal-Ezer, H. *Chem. Phys. Lett.* 1986, **127**: 233.

(41) Kosloff, R. *J. Phys. Chem.* 1988, **92**: 2087.

(42) Benjamin, I.; Banin, U.; Ruhman, S. *J. Chem. Phys.* 1983, **98**: 8337.

(43) Benjamin, I. Gertner, B.J.; Tang, N.J.; Wilson, K.R. *J. Am. Chem. Soc.* 1990, **112**: 524; Gertner, B.J.; Whitnell, R.M.; Wilson, K.R.; Hynes, J.T. ibid 1991, **113**: 74.